

Carbothermic reduction of vanadium titanomagnetite with the assistance of sodium carbonate

Luming Chen^{1,2)}, Yulan Zhen^{1,✉}, Guohua Zhang³⁾, Desheng Chen¹⁾, Lina Wang¹⁾, Hongxin Zhao¹⁾, Fancheng Meng¹⁾, and Tao Qi¹⁾

1) National Engineering Laboratory for Hydrometallurgical Cleaner Production Technology, Institute of Process Engineering, Beijing 100190, China

2) School of Chemical Engineering, University of Chinese Academy of Sciences, Beijing 100190, China

3) State Key Laboratory of Advanced Metallurgy, University of Science and Technology Beijing, Beijing 100083, China

(Received: 29 May 2020; revised: 5 August 2020; accepted: 7 August 2020)

Abstract: The carbothermic reduction of vanadium titanomagnetite concentrate (VTC) with the assistance of Na_2CO_3 was conducted in an argon atmosphere between 1073 and 1473 K. X-ray diffraction and scanning electron microscopy were used to investigate the phase transformations during the reaction. By investigating the reaction between VTC and Na_2CO_3 , it was concluded that molten Na_2CO_3 broke the structure of titanomagnetite by combining with the acidic oxides (Fe_2O_3 , TiO_2 , Al_2O_3 , and SiO_2) to form a Na-rich melt and release FeO and MgO. Therefore, Na_2CO_3 accelerated the reduction rate. In addition, adding Na_2CO_3 also benefited the agglomeration of iron particles and the slag–metal separation by decreasing the viscosity of the slag. Thus, Na_2CO_3 assisted carbothermic reduction is a promising method for treating VTC at low temperatures.

Keywords: vanadium titanomagnetite; sodium carbonate; phase transformation; carbothermic reduction; slag–metal separation

1. Introduction

Vanadium titanomagnetite concentrate (VTC), containing several valuable metallic elements, is a type of complex iron ore. In China, approximately 9.66 billion tons of VTC is located in the Panzhihua-Xichang region [1]. The titanium resources in this region account for approximately 95% of the entire titanium resources in China and approximately 54% of the titanium resources in VTC after physical separation [2]. Thus, the efficient and comprehensive use of VTC is a hot research topic.

At present, the traditional blast furnace process [3] and direct reduction–electric furnace smelting (or magnetic separation) [1,4–7] are the two main methods for smelting VTC. However, these two processes, whose principle is essentially the carbothermal reduction of VTC, still have technological problems. In the blast furnace process, the Ti(C,N) phase is easily generated, whereas the formed Ti(C,N) particles cause an increase in the viscosity of the slag and in the difficulty in separating the iron from slag because of the good wettability with molten slags [1,8]. To reduce the probability of generating the Ti(C,N) phase during smelting, ordinary iron ores are blended with VTC. However, these operations reduce the concentration of TiO_2 in the slag and make recycling TiO_2 very difficult [9–10]. Compared to the blast furnace process,

after the direct reduction process, the content of titania in the products is much higher, but the problems of iron–slag separation and direct utilization of the titanium-rich phase has not been solved effectively [5–6].

Recently, our group proposed a new carbothermic reduction method with the assistance of alkali (Na_2CO_3 or NaOH) to reduce VTC at low temperatures (~1473 K) [11–13]. In this process, in the obtained titanium-rich slag, titanium is mainly present in different sodium titanates. Because the sodium (Na^+) in the sodium titanate crystal is easily exchanged with H^+ , the highly active, titanium-rich slag can be effectively treated by an acid leaching process [14–15]. However, the effects of Na_2CO_3 addition and the reaction mechanism of this process, which are the subjects of this study, have not been systematically investigated.

Many related studies on the carbothermal reduction process of iron ore with the addition of Na_2CO_3 have been conducted. Chen *et al.* [16] found that the crystal lattice of raw VTC was destroyed and pores were formed after adding Na_2CO_3 , which accelerated the reduction process and reduced the reaction temperature. Another proposed effect was that alkaline additives promote the reduction process by catalyzing a carbon–gas reaction (Boudoir reaction) [17–18]. However, the added amounts of Na_2CO_3 in their work were low (<5wt%), and Na_2CO_3 did not directly participate in the

✉ Corresponding author: Yulan Zhen E-mail: zhenzhen9545@126.com

© University of Science and Technology Beijing 2022

reaction. When the additive amount of Na_2CO_3 increased, its interaction with the ore could not be ignored. Some investigations were conducted on the interaction mechanism of Na_2CO_3 and ilmenite during the roasting process [19–21], and it was concluded that Na_2CO_3 can react with ilmenite at above 1123 K to generate various binary ferrite, titanate, and ternary $\text{Na}_2\text{O}\text{--}\text{Fe}_2\text{O}_3\text{--}\text{TiO}_2$ phases [22–23]. However, no clear description of microstructure evolution in the reaction process was provided. Hence, the reaction mechanism between Na_2CO_3 and VTC remains unclear and must be illustrated. In the present study, the carbothermic reduction reaction of VTC with the assistance of Na_2CO_3 is investigated in detail to elucidate the effect of Na_2CO_3 during the reaction process. In addition, the optimal reaction parameters are studied.

2. Experimental

2.1. Raw materials

Vanadium titanomagnetite concentrate was obtained from the Panzhihua Iron & Steel Company, China, with the chemical composition shown in Table 1. The total iron content (TFe), FeO content, and TiO_2 content were determined using the chemical titration method, while the content of Fe_2O_3 was calculated as the difference between the total iron and FeO contents. The contents of other components were examined using X-ray fluorescence (ShimadzuXRF-1800, current 140 mA, voltage 60 kV). The X-ray diffraction (XRD) patterns of VTC are shown in Fig. 1, from which it is apparent that the main mineral phase of VTC was titanomagnetite ($\text{Fe}_{3-x}\text{Ti}_x\text{O}_4$), with the presence of a small amount of ilmenite (FeTiO_3) and pyroxene (Mg_2SiO_4). The reagent grade graphite and Na_2CO_3 were purchased from the Sinopharm Chemical Reagent Co., Ltd., China.

Table 1. Chemical composition of vanadium titanium magnetite concentrate

	TFe	Fe_2O_3	FeO	TiO_2	SiO_2	CaO	Al_2O_3	MgO	V_2O_5	Others
	53.99	43.28	30.51	12.24	1.98	0.95	4.54	5.2	0.53	0.77

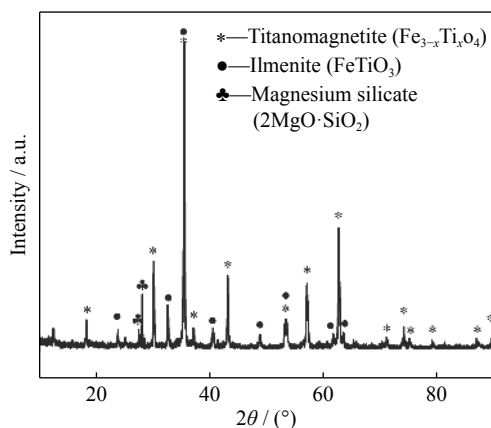
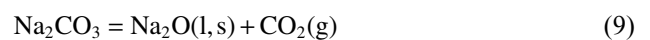
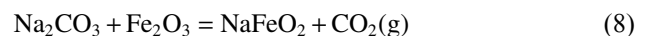
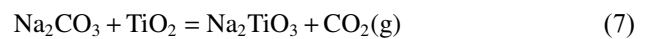
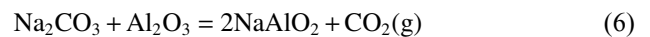
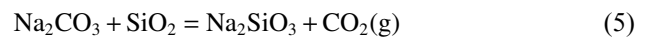
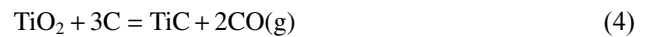


Fig. 1. XRD patterns of vanadium titanium magnetite concentrate.

2.2. Experimental procedure

Based on the work of Zhang *et al.* [12], a high vanadium extraction rate and good slag-iron separation effect were achieved when the Na_2CO_3 -to-VTC mass ratio ($R_{N/V}$) was 60%. Therefore, herein, $R_{N/V}$ was also set to 60%. The mass ratio of C-to-VTC ($R_{C/V}$) was calculated as follows. According to the main components of the vanadium titanomagnetite concentrate (shown in Table 1), in the $\text{Na}_2\text{CO}_3\text{--C--VTC}$ system, the possible reactions may include reductions of iron oxides or titanic oxide (Eqs. (1)–(4)), reactions between the acidic oxides (SiO_2) or amphoteric oxides (Al_2O_3 , TiO_2 , Fe_2O_3) in VTC and Na_2CO_3 (Eqs. (5)–(8)), thermal decomposition of Na_2CO_3 (Eq. (9)), carbothermic reduction of Na_2CO_3 (Eqs. (9) and (10)), and a carbon gasification reaction (Eq. (11)) [24].



The standard Gibbs free energy changes of different reactions were calculated using Factsage 7.0 [25] and the results are shown in Fig. 2. The graphs of Eqs. (1)–(4) and (10) in Fig. 2(a) indicate that the critical temperatures (corresponding to the value at which $\Delta G_T^\ominus = 0$ kJ/mol) for carbothermic reduction of different components follow the sequence $T_{\text{FeO}} < T_{\text{Na}_2\text{O}} < T_{\text{TiO}_2}$. The graphs of Eqs. (3) and (4) indicate that the temperature for the reduction of TiO_2 to TiC (1562 K) is lower than that to metallic Ti (2038 K). To guarantee the reduction of iron oxides and avoid the generation of TiC, the temperature range of the experiment was set as 1073–1473 K. In addition, based on Fig. 2(b), it can also be concluded that the reactions between Na_2CO_3 and acidic/amphoteric oxides (Eqs. (5)–(8)) may occur at the current experimental temperature. Furthermore, Fig. 2(b) shows that Na_2O can be reduced by C when the reaction temperature exceeds 1286 K. The critical temperature will be even lower in the actual experiment because of the use of Ar as the protecting gas, which decreases the partial pressure of the gaseous product. Kim and Lee [24] also concluded that Na_2O can be reduced when the temperature exceeded the melting point of Na_2CO_3 (~1123 K). Therefore, the carbothermic reduction of Na_2O should be addressed.

The computed Gibbs free energy changes for the reactions in Fig. 3 involving TiO_2 show that, if only the reduction of TiO_2 is considered, the phases of TiO_{2n-1} will be generated.

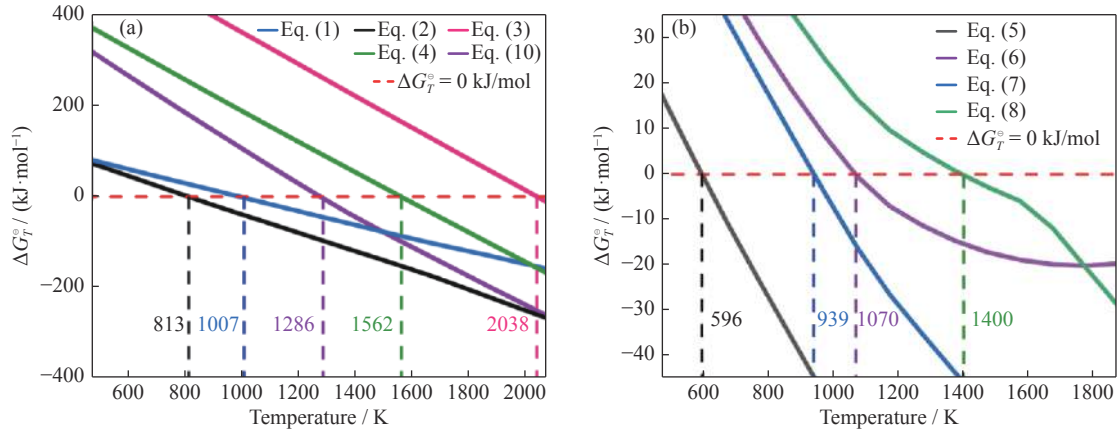


Fig. 2. Standard Gibbs free energy change as a function of temperature: (a) carbothermic reduction reactions (Eqs. (1)–(4) and (10)); (b) reactions between the oxides in VTC and Na_2CO_3 (Eqs. (5)–(8)).

However, in the present study, the slag was composed of composite mineral phases, and the reduction of titanates (Na_2TiO_3 , CaTiO_3 , and Mg_2TiO_4) was much more difficult than that of TiO_2 at 1073–1473 K based on the thermodynamic calculations shown in Fig. 3. Hence, the presence of low valence Ti in the slag is negligible.

The volume fractions of the CO and CO_2 produced during the reduction process when the mass ratio of C-to-VTC ($R_{C/V}$) was 25% were detected using an infrared gas analyzer and are shown in Fig. 4, from which it is obvious that the main gaseous product in the reaction process was CO. Therefore, to predetermine the amount of added carbon, for simplicity, only the gaseous product of CO was considered.

Assuming the main gaseous product is CO, the theoretical minimum of $R_{C/V}$ (R_{\min}) can be calculated using Eq. (12) if only the reduction of iron oxides is considered (Eqs. (1) and (2)). Its maximum (R_{\max}) can be calculated using Eq. (13) because of Eqs. (9)–(11).

$$R_{\min} = m_{\text{FeO}} \times \frac{12}{72} + m_{\text{Fe}_2\text{O}_3} \times \frac{36}{160} \quad (12)$$

$$R_{\max} = R_{\min} + R_{N/V} \times \frac{24}{106} \quad (13)$$

where m_{FeO} and $m_{\text{Fe}_2\text{O}_3}$ are mass fractions of FeO and Fe_2O_3 in titanomagnetite (shown in Table 1). R_{\min} and R_{\max} are calcu-

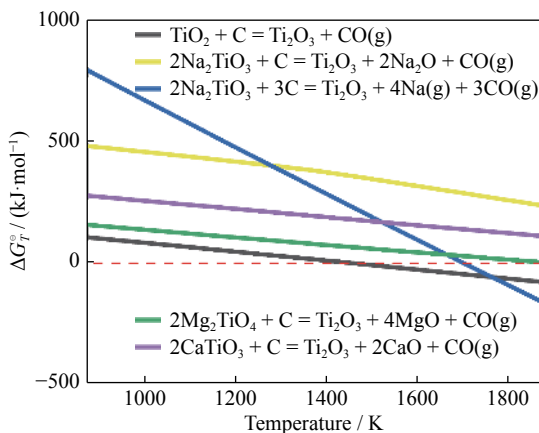


Fig. 3. Variations in the standard Gibbs free energy change for the reduction reactions involving TiO_2 .

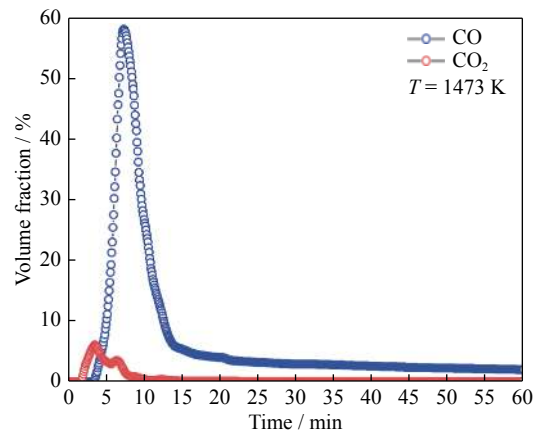


Fig. 4. Volume fractions of CO and CO_2 in the gaseous product generated in the isothermal reduction process of VTC at 1473 K when the mass ratio of Na_2CO_3 to VTM was 60%.

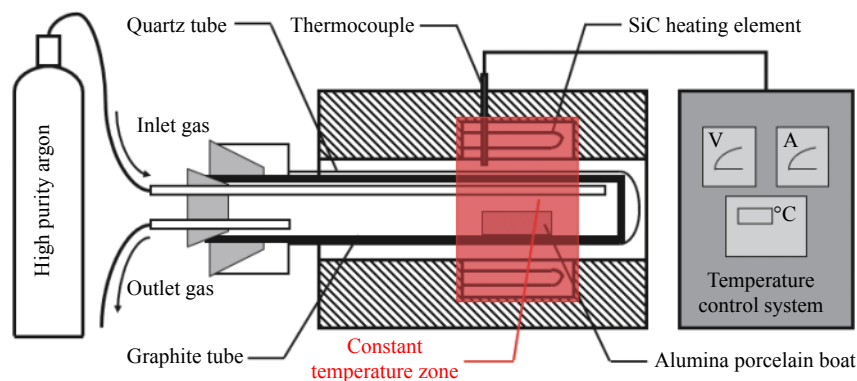
lated to be 14.88% and 28.44%, respectively. Accordingly, $R_{C/V}$ was set to 15%, 20%, 25%, and 29% to study with the influence of carbon content on the reaction process.

To simplify the description, herein, the sample name is referred to as “XC_YN_t_T,” with a certain mass ratio (X/Y/100) of graphite (C), Na_2CO_3 (N), and VTC, at the reaction temperature T K for t h. A summary of the experimental conditions in this study can be found in Table 2.

A schematic diagram of the experimental apparatus is shown in Fig. 5. A horizontal tube furnace with silicon carbide rod heating elements was used. The diameter of the quartz tube was 48 mm and the length of the constant temperature zone of the furnace was 60 mm. A graphite tube with one end sealed was used to protect the quartz tube from corrosion at high temperatures due to the generation of Na vapor. The raw materials (10 g) were first ground in an agate mortar for 30 min and then transferred to an alumina boat (60 mm \times 15 mm \times 15 mm). The alumina boat was put in the graphite inner tube embedded in the quartz tube, which was then placed in the constant temperature zone of the furnace. Argon gas (0.3 L/min) was blown for 1 h in advance to exclude the air from the graphite tube. When the furnace temperature reached the desired value, the quartz tube was quickly inserted into the furnace. After reacting for a certain

Table 2. Experimental conditions of sodium carbonate assisted carbon thermal reduction of titanium magnetite

Sample (XC_YN_t_T)	Composition		Reaction time, t / h	Reaction temperature, T / K
	R_{CV} / % (X)	R_{NV} / % (Y)		
15C_60N_2_1473	15	60	2	1473
20C_60N_2_1473	20	60	2	1473
25C_60N_2_1473	25	60	2	1473
29C_60N_2_1473	29	60	2	1473
25C_60N_2_1073	25	60	2	1073
25C_60N_2_1273	25	60	2	1273
25C_60N_1_1473	25	60	1	1473
25C_60N_0.5_1473	25	60	0.5	1473
25C_60N_0.25_1473	25	60	0.25	1473
0C_60N_2_1473	0	60	2	1473
25C_0N_2_1473	60	0	2	1473

**Fig. 5. Schematic diagram of the experimental apparatus.**

time, the quartz tube was rapidly removed from the furnace and cooled to room temperature in a flowing argon atmosphere.

After cooling, the generated iron beads were separated from the slag. The phase composition of the reduced sample was examined via XRD (TTR III, conducted using a Cu K_{α} source, tube current of 10–300 mA, tube voltage of 20–60 kV) in the 2θ range from 10° to 90° with a scanning rate of $15^{\circ}/\text{min}$. The morphology was characterized using scanning electron microscopy (SEM) (Quanta 250, FEI Company, US). Notably, considering the degree of hydration of high sodium oxide slag, the method of dry grinding and dry polishing was adopted in this study. The volume fractions of CO and CO_2 were recorded by an infrared gas analyzer (XLZ-1090) every 5 s during the reaction process until their values decreased to 0.1%.

3. Results

3.1. Total mass loss ratio

During the carbothermic reduction process of VTC with the assistance of Na_2CO_3 , the total mass loss ratios (W) in the experiments were calculated using Eq. (14):

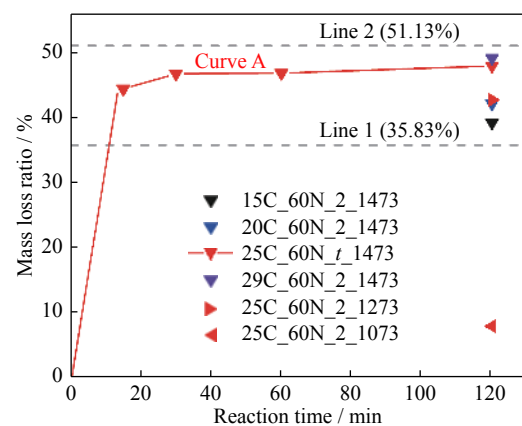
$$W = \frac{w_0 - w_t}{w_0} \times 100\% \quad (14)$$

where w_0 is the initial mass of the sample, and w_t is the mass

of the sample after reaction time t .

The total mass loss ratio W of the relevant samples is shown in Fig. 6. Line 1 ($W = 35.83\%$) and Line 2 ($W = 51.13\%$) show the theoretical mass loss ratios when R_{CV} was 14.88% and 28.44%, respectively. Samples with different R_{CV} (15%, 20%, 25%, and 29%) have W values located between Line 1 and Line 2, which explains why some Na_2O was reduced by carbon during this process.

Furthermore, the greater the amount of added carbon was, the larger the value of W was, because more Na_2O was re-

**Fig. 6. Mass loss ratios of different samples after reacting at different temperatures for different times.**

duced as the amount of carbon increased. In addition, by comparing the mass loss ratios of the samples (25C_60N_2_1073, 25C_60N_2_1273, and 25C_60N_2_1473), it can be concluded that the reaction rate increased with temperature. Moreover, curve A distinctly shows that the carbothermic reduction reaction was very fast with the assistance of Na_2CO_3 , and the reduction reaction was almost completed after 30 min.

3.2. Phase transformation

The detected phase compositions of the samples XC_60N_2_1473 with various R_{CV} after reacting at 1473 K for 2 h are shown in Fig. 7. When R_{CV} was 15% and 20%, the main phases of the products were the $\text{Na}_2\text{O}-\text{Fe}_2\text{O}_3-\text{TiO}_2$ ternary compound ($\text{Na}_{0.75}\text{Fe}_{0.75}\text{Ti}_{0.25}\text{O}_2$), magnesium iron oxides ($\text{MgO}_{0.239}\text{FeO}_{0.761}$ or $\text{MgO}_{0.77}\text{FeO}_{0.23}$), iron (Fe), and sodium aluminum silicate ($\text{Na}_{1.95}\text{Al}_{1.95}\text{Si}_{0.05}\text{O}_4$). This result indicates that some iron oxides in VTC were reduced, but unreduced iron oxides remained in the slag (e.g., $\text{Na}_{0.75}\text{Fe}_{0.75}\text{Ti}_{0.25}\text{O}_2$ and $\text{MgO}_{0.77}\text{FeO}_{0.23}$).

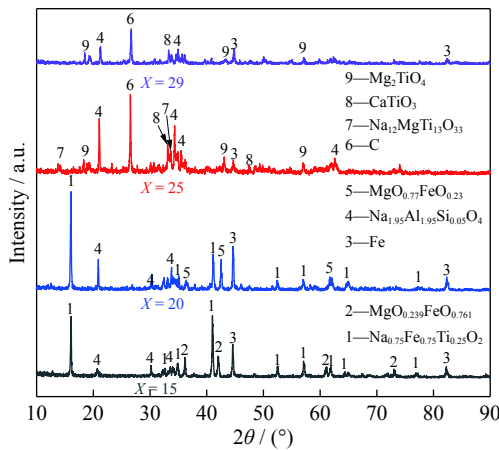


Fig. 7. XRD patterns of the products reduced at 1473K for 2 h with different amounts of graphite (XC_60N_2_1473, X = 15, 20, 25, and 29).

Meanwhile, during the reaction process, many sodium ions destroyed the mineral phases of VTC and formed a liquid phase, such as $\text{Na}_{1.95}\text{Al}_{1.95}\text{Si}_{0.05}\text{O}_4$. As R_{VC} increased to 25%, the characteristic peaks of sodium iron titanium oxide and magnesium iron oxides disappeared, but the peaks of graphite appeared because the amount of graphite was excessive and sufficient to reduce all iron oxides in the VTC. The phase components of the products (after separating the iron) were the $\text{Na}_2\text{O}-\text{MgO}-\text{TiO}_2$ ternary compound ($\text{Na}_{12}\text{MgTi}_{13}\text{O}_{33}$), perovskite (CaTiO_3), and magnesium–titanium spinel (Mg_2TiO_4). Upon increasing R_{CV} to 29%, $\text{Na}_{12}\text{MgTi}_{13}\text{O}_{33}$ disappeared because more Na_2O in the melt was reduced by graphite. However, reducing the TiO_2 in CaTiO_3 and Mg_2TiO_4 was difficult because of their stable crystalline structures [6,11]. Therefore, a R_{CV} of 25% was adopted for further experiments.

Fig. 8 shows the XRD patterns of the products for the samples (25C_60N_2_T) after reacting at 1073, 1273, and 1473 K. At 1073 K, the $\text{Na}_2\text{O}-\text{Fe}_2\text{O}_3-\text{TiO}_2$ ternary com-

pound ($\text{Na}_{0.75}\text{Fe}_{0.75}\text{Ti}_{0.25}\text{O}_2$) was generated, accompanied by the formation of FeO. When the reduction temperature was increased to 1273 K, the Na_2CO_3 , titanomagnetite, and $\text{Na}_{0.75}\text{Fe}_{0.75}\text{Ti}_{0.25}\text{O}_2$ phases almost disappeared, while sodium titanate ($\alpha\text{-Na}_2\text{TiO}_3$ [14]) and iron (Fe) became apparent. This result indicated that most iron oxides were reduced to metallic iron, except those in the stable $\text{MgO}_{0.77}\text{FeO}_{0.23}$ solid phase. As the reaction temperature was further increased to 1473 K, all iron oxides were reduced to metallic iron, and the sodium titanate phase transformed into the $\text{Na}_2\text{O}-\text{MgO}-\text{TiO}_2$ ternary compound ($\text{Na}_{12}\text{MgTi}_{13}\text{O}_{33}$), perovskite (CaTiO_3), and magnesium–titanium spinel (Mg_2TiO_4). Meanwhile, the diffraction peak intensity of metallic iron (Fe) became weak, suggesting that the separation between iron and slag was better at 1473 K. Consequently, the proper temperature was 1473 K.

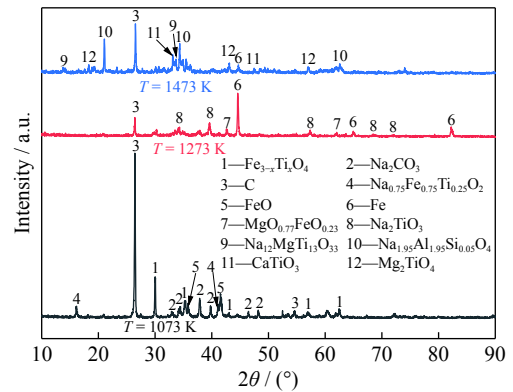


Fig. 8. XRD patterns of the products for samples 25C_60N_2_T (T = 1073, 1273, and 1473 K).

The XRD patterns of the products for the samples (25C_60N_t_1473) reduced for various times are shown in Fig. 9, and the identified phases are listed in Table 3. The $\text{Na}_2\text{O}-\text{Fe}_2\text{O}_3-\text{TiO}_2$ ternary compounds (e.g., $\text{Na}_{0.75}\text{Fe}_{0.75}\text{Ti}_{0.25}\text{O}_2$ and NaFeTiO_4) were identified after reacting for 1 h. However, after 2 h, the diffraction peaks of the ternary compounds disappeared. This phenomenon indicated that some ferric ions in the slag phase were reduced by graphite. Meanwhile, with the increase in reaction time, the relative intensity of the diffraction peaks of iron decreased and nearly disappeared after 2 h, indicating the effective separation of the

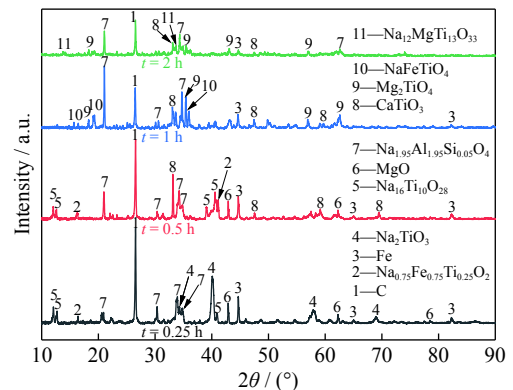
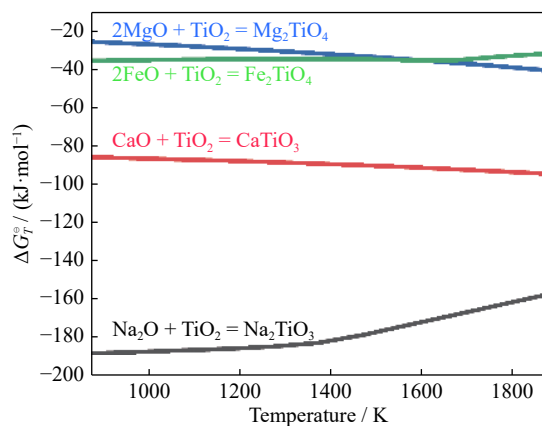


Fig. 9. XRD patterns of the products for the samples 25C_60N_t_1473 (t = 0.25, 0.5, 1, and 2 h).

Table 3. Phase compositions of the products for the samples 25C_60N_t_1473

Sample	Identified phases
25C_60N_0.25_1473	C, Fe, Na _{0.75} Fe _{0.75} Ti _{0.25} O ₂ , Na ₂ TiO ₃ , Na ₁₆ Ti ₁₀ O ₂₈ , Na _{1.95} Al _{1.95} Si _{0.05} O ₄ , MgO
25C_60N_0.5_1473	C, Fe, Na _{0.75} Fe _{0.75} Ti _{0.25} O ₂ , Na ₁₆ Ti ₁₀ O ₂₈ , Na _{1.95} Al _{1.95} Si _{0.05} O ₄ , MgO
25C_60N_1_1473	C, Fe, NaFeTiO ₄ , CaTiO ₃ , Mg ₂ TiO ₄ , Na _{1.95} Al _{1.95} Si _{0.05} O ₄
25C_60N_2_1473	C, Fe, Na ₁₂ MgTi ₁₃ O ₃₃ , CaTiO ₃ , Mg ₂ TiO ₄ , Na _{1.95} Al _{1.95} Si _{0.05} O ₄

slag and iron. Moreover, as the reaction proceeded, the phase containing sodium and titanium changed from α -Na₂TiO₃ to Na₁₆Ti₁₀O₂₈ and then to Na₁₂MgTi₁₃O₃₃, CaTiO₃, and Mg₂TiO₄. According to the changes in standard Gibbs free energy of the reactions between basic oxides (Na₂O, CaO, MgO, and FeO) and TiO₂ shown in Fig. 10, it is much easier for Na₂O to react with TiO₂. However, Na₂O is continuously consumed by graphite during the smelting process, so the other titanates may also be generated when the amount of Na₂O is not sufficient.

**Fig. 10. Variations in the standard Gibbs free energy changes of the reduction reactions between basic oxides and TiO₂.**

3.3. Microstructure evolution

To further analyze the reaction process, the microstructures of the samples reduced with different R_{CV} values, temperatures, and time periods were detected and are shown in Fig. 11. As shown in Fig. 11(a), metallic iron particles and slag were in the products. The iron particles were agglomerated, and the slag contained four major regions, namely, Na₁₂MgTi₁₃O₃₃, Na_{1.95}Al_{1.95}Si_{0.05}O₄, CaTiO₃, and Mg₂TiO₄ phases. In addition, no iron element was present in the slag phases, which indicated that all the iron was metallized.

In Fig. 11(b), only the slag phase was present because iron particles were separated during the grinding and polishing process. In the slag phase, regions 5–7 was represented as MgO_{0.77}FeO_{0.23}, Na_{0.75}Fe_{0.75}Ti_{0.25}O₂, and Na_{1.95}Al_{1.95}Si_{0.05}O₄, respectively. The results showed that abundant Fe₂O₃ remained in the slag phase because of the insufficient graphite addition.

The microstructure of 25C_60N_2_1273 is shown in Fig. 11(c), which indicated that the main phase (region 8) was sodium titanate (α -Na₂TiO₃). The small metallic iron particles were dispersively distributed in the reduced products, so separating iron from slag was difficult. Fig. 9(d) shows the mi-

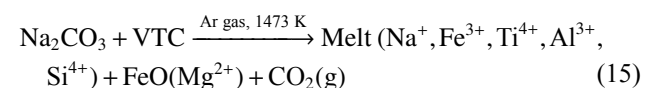
crostructure of the sample 15C_60N_0.5_1473. Except for the iron phase, the slag phase was composed of four regions, namely, Na₁₆Ti₁₀O₂₈, Na_{1.95}Al_{1.95}Si_{0.05}O₄, CaTiO₃, and Na_{0.75}Fe_{0.75}Ti_{0.25}O₂, corresponding to Regions 9–12, respectively. Therefore, unreduced iron oxides remained in the slag after reaction for 30 min.

From the above results, it can be concluded that the phase compositions obtained from the energy dispersive X-ray spectroscopy (EDS) analyses were consistent with those of the XRD analysis. Meanwhile, the iron oxide in sample 25C_60N_2_1473 was completely reduced and had a good separation effect with slag.

4. Discussion

4.1. Reaction mechanism of VTC with Na₂CO₃

The reaction between Na₂CO₃ and VTC is of great importance for the carbothermic reduction process of VTC, and it is necessary to investigate its reaction mechanism. Fig. 12(a) and (b) are the XRD and SEM-EDS results, respectively, of the products for sample 0C_60N_2_1473. Fig. 12(a) shows that the main phases of roasted products were the Na₂O-Fe₂O₃-TiO₂ ternary compound (Na_{0.75}Fe_{0.75}Ti_{0.25}O₂), ferrous oxide (FeO), and the Na₂O-Al₂O₃-SiO₂ ternary compound (Na_{1.95}Al_{1.95}Si_{0.05}O₄). Fig. 12(b) shows that the roasted product was composed of three phases, which was consistent with the results of XRD. Interestingly enough, the regions of the three phases formed a nucleus-like structure, with the solid solution phase of FeO and MgO (region 1) in the center and the ternary compounds (regions 2 and 3) at the edges. The formation of this structure was beneficial for the reduction reaction. It may be inferred that the Na₂CO₃ melt broke and entered into the lattices of VTC to form a complex melt with the acidic oxides (Fe₂O₃, TiO₂, Al₂O₃, and SiO₂) because Na₂O is a basic oxide, while some basic oxides (FeO and MgO) were released. Holloway *et al.* [26–27] reported the similar result that ZnFe₂O₄ spinel transformed into ZnO and either α -NaFeO₂ or β -NaFeO₂ in the presence of Na₂CO₃. Selivanov *et al.* [28] also confirmed that Na₂CO₃ can replace FeO and MnO in wolframite. Therefore, the reaction mechanism between Na₂CO₃ and VTC can be described as Eq. (15):



As the reaction proceeded, more acidic oxides diffused to the edge of the melt and combined with Na₂O to form different compounds (during cooling), with FeO and MgO remaining in the center to form the core phase.

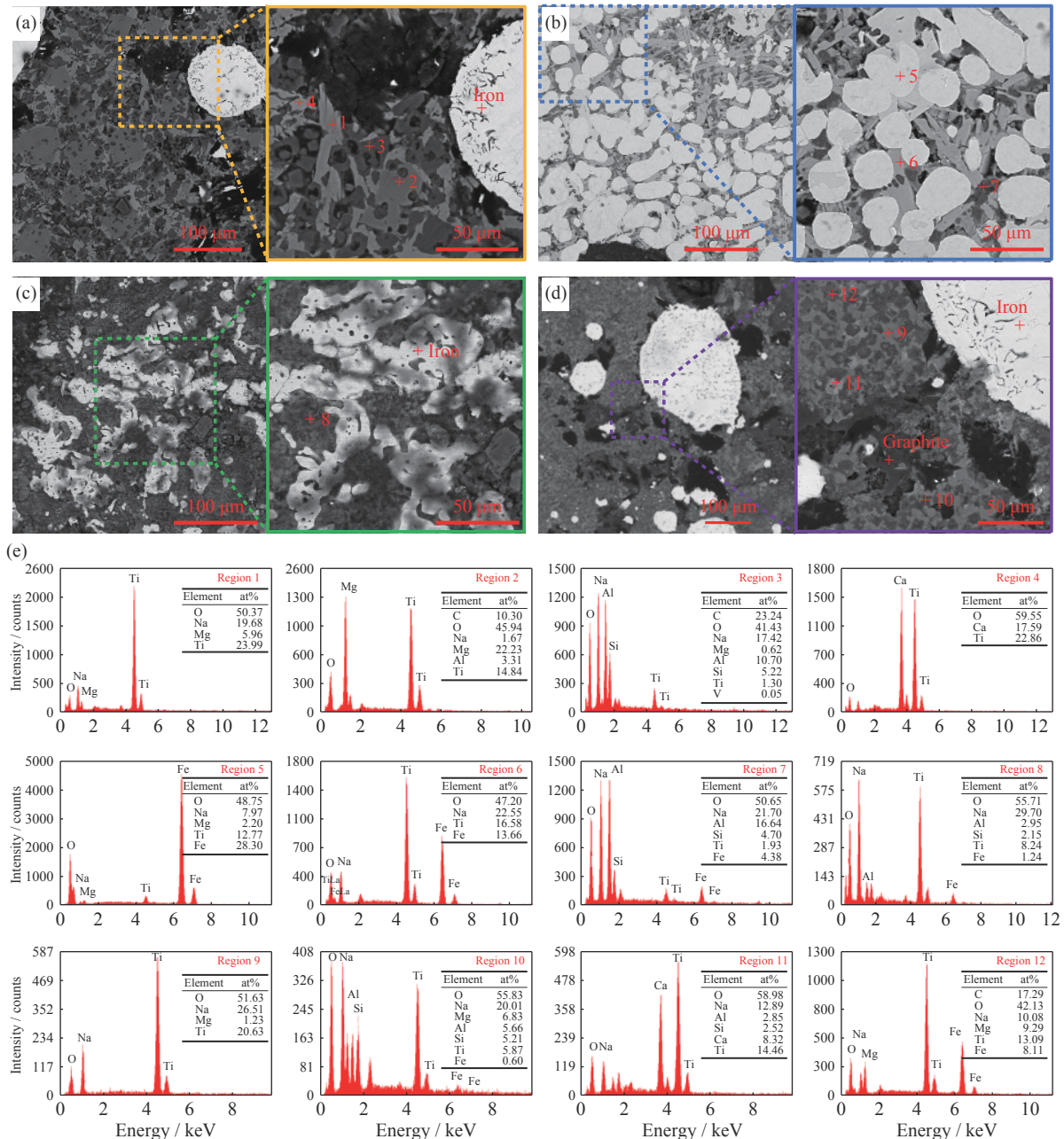


Fig. 11. SEM images of the samples: (a) 25C_60N_2_1473; (b) 20C_60N_2_1473; (c) 25C_60N_2_1273; (d) 25C_60N_0.5_1473; and (e) EDS analysis results of the corresponding regions.

4.2. Effect of Na_2CO_3 on the reduction process

The microstructures of the reduced samples of 25C_0N_2_1473 (without the addition of Na_2CO_3) and 25C_60N_2_1473 are shown in Fig. 13. For 25C_0N_2_1473, the generated iron was dispersed and embedded in the slag, which increased the difficulty of separation. For 25C_60N_2_1473, the iron phase agglomerated in beads and was separated effectively from the slag. These phenomena indicated that Na_2CO_3 helped iron particles to grow and separate from the slag because of the generation of the liquid slag and the decrease in the viscosity of liquid slag [29]. In addition, the volume fraction changes in CO generated during the reduction process (shown in Fig. 14) clearly indicate that the reaction rate of 25C_60N_2_1473 was much faster than that of 25C_0N_2_1473, which, in turn, indicates that Na_2CO_3 ac-

celerated the reducing reaction. The reason for the acceleration may be related to the catalytic effect of Na_2CO_3 on the carbon-gas reaction [30] and the destruction of mineral structures by Na_2CO_3 [16].

4.3. Carbothermic reduction mechanism

Fig. 11(d) shows that the product of sample 25C_60N_0.5_1473 contained the $\text{Na}_2\text{O}-\text{Fe}_2\text{O}_3-\text{TiO}_2$ ternary phase ($\text{Na}_{0.75}\text{Fe}_{0.75}\text{Ti}_{0.25}\text{O}_2$), which confirmed that Fe_2O_3 entered the melt during the reduction process. Moreover, after 2 h of reduction of sample 15C_60N_2_1473, no Fe oxide was present in the slag. Therefore, the Fe_2O_3 in the melt had been reduced completely. Accordingly, two mechanisms were proposed for the reduction of iron oxide in VTC: direct reduction by graphite and reduction from liquid slag. The latter

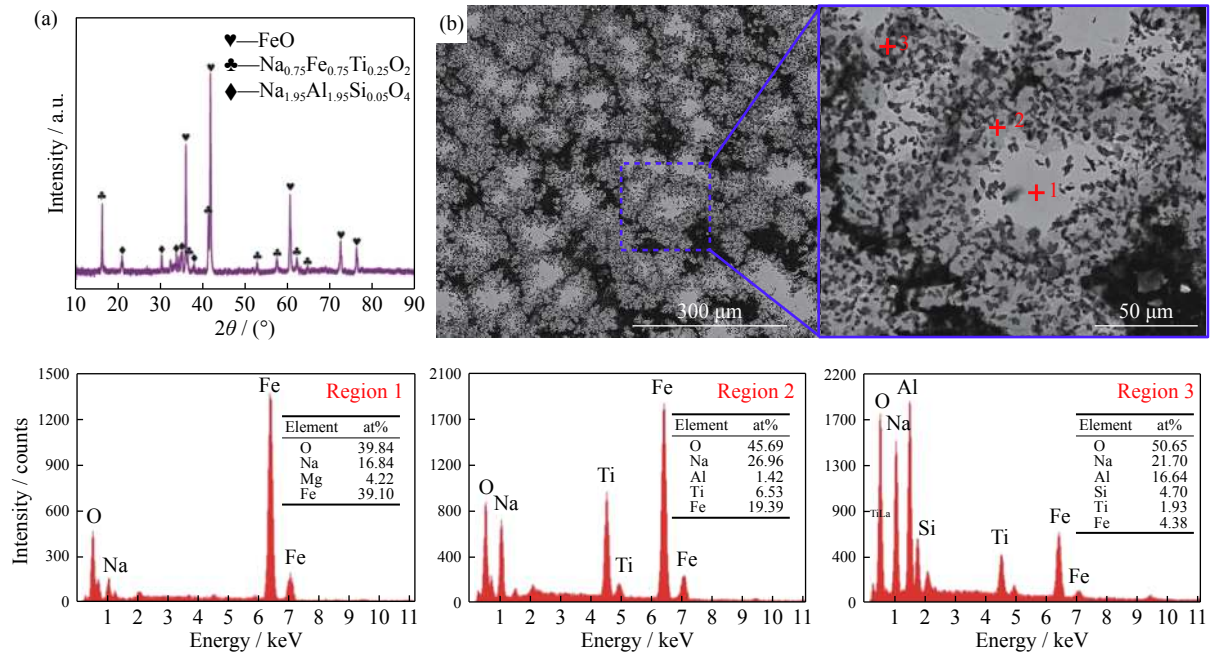


Fig. 12. XRD pattern (a) and SEM-EDS results (b) of sample 0C_60N_2_1473.

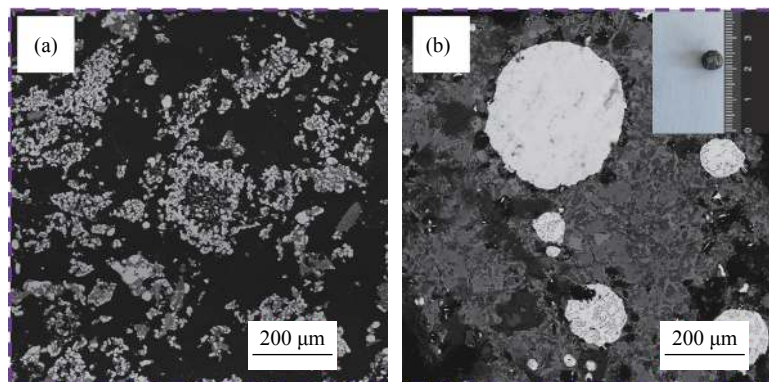


Fig. 13. SEM images of (a) 25C_0N_2_1473 and (b) 25C_60N_2_1473. Inset: example of the separated iron bread.

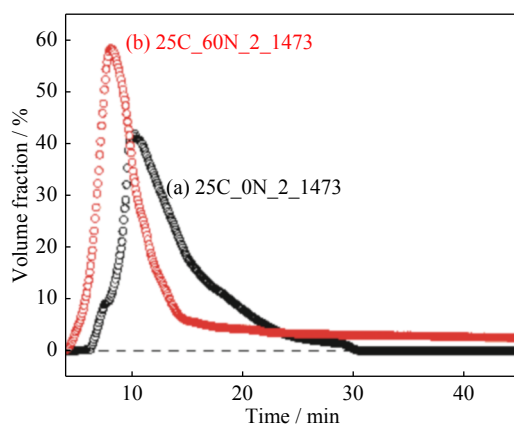


Fig. 14. Examples of the volume fraction of carbon monoxide at 1473 K: (a) 25C_0N_2_1473 and (b) 25C_60N_2_1473.

mechanism involved a solid (graphite)–liquid (melt) reaction. The activity of iron oxide gradually decreases in the liquid slag as the reaction proceeds, which is bad for the reduction reaction. The reaction time increases compared with that without Na₂CO₃, as indicated by Fig. 14. This phenomenon is consistent with the conclusion of Pan *et al.* [31] that suffi-

cient Na₂O retarded the reduction of Fe₂O₃ because the formed liquid phase inhibited the diffusion of the reducing gases.

5. Conclusions

The present study investigated the carbothermal reduction process of vanadium titanomagnetite with the assistance of Na₂CO₃ under an argon atmosphere, and the following conclusions were reached.

(1) The optimal mass ratio of VTC : C : Na₂CO₃ was 100:25:60 at 1473 K.

(2) During the reaction of Na₂CO₃ with VTC, acidic oxides (Fe₂O₃, TiO₂, Al₂O₃, and SiO₂) in VTC entered molten Na₂CO₃ to form a Na-rich melt, and the residual basic oxides (FeO and MgO) were concentrated in the center to form a solid solution phase.

(3) During the reduction process, Na₂CO₃ not only accelerated the reduction rate but also promoted the separation of generated iron from slag by decreasing the viscosity of the slag.

Acknowledgements

This work was financially supported by the National Key R&D Program of China (No. 2018YFC1900500), the National Natural Science Foundation of China (Nos. 21908231, 51774260, 51804289, and 51904286), the Key Research Program of Frontier Sciences of the Chinese Academy of Sciences (No. QYZDJ-SSW-JSC021), the CAS Interdisciplinary Innovation Team, and the Special Project for Transformation of Major Technological Achievements in Hebei Province, China (No. 19044012Z).

Conflict of Interests

The authors declared that they do not have any commercial or associative interest that represents a conflict of interest in connection with the work submitted

References

- [1] F. Zheng, F. Chen, Y. Guo, T. Jiang, A. Y. Travyanov, and G. Qiu, Kinetics of hydrochloric acid leaching of titanium from titanium-bearing electric furnace slag, *JOM*, 68(2016), No. 5, p. 1476.
- [2] X.W. Lv, Z.Q. Lun, J.Q. Yin, and C.Q. Bai, Carbothermic reduction of vanadium titanomagnetite by microwave irradiation and smelting behavior, *ISIJ Int.*, 53(2013), No. 7, p. 1115.
- [3] S. Wang, Y.F. Guo, T. Jiang, L. Yang, F. Chen, F.Q. Zheng, X.L. Xie, and M.J. Tang, Reduction behaviors of iron, vanadium and titanium oxides in smelting of vanadium titanomagnetite metallized pellets, *JOM*, 69(2017), No. 9, p. 1646.
- [4] S. Samanta, S. Mukherjee, and R. Dey, Upgrading metals via direct reduction from poly-metallic titaniferous magnetite ore, *JOM*, 67(2015), No. 2, p. 467.
- [5] M.Y. Wang, S.F. Zhou, X.W. Wang, B.F. Chen, H.X. Yang, S.K. Wang, and P.F. Luo, Recovery of iron from chromium vanadium-bearing titanomagnetite concentrate by direct reduction, *JOM*, 68(2016), No. 10, p. 2698.
- [6] Y.Q. Zhao, T.C. Sun, H.Y. Zhao, C. Chen, and X.P. Wang, Effect of reductant type on the embedding direct reduction of beach titanomagnetite concentrate, *Int. J. Miner. Metall. Mater.*, 26(2019), No. 2, p. 152.
- [7] X.H. Li, J. Kou, T.C. Sun, S.C. Wu, and Y.Q. Zhao, Effects of calcium compounds on the carbothermic reduction of vanadium titanomagnetite concentrate, *Int. J. Miner. Metall. Mater.*, 27(2020), No. 3, p. 301.
- [8] Y.L. Zhen, G.H. Zhang, and K.C. Chou, Viscosity of CaO–MgO–Al₂O₃–SiO₂–TiO₂ melts containing TiC particles, *Metall. Mater. Trans. B*, 46(2015), p. 155.
- [9] W.Q. Fu, Y.C. Wen, and H.E. Xie, Development of intensified technologies of vanadium-bearing titanomagnetite smelting, *J. Iron. Steel. Res. Int.*, 18(2011), No. 4, p. 7.
- [10] L. Zhang, L.N. Zhang, M.Y. Wang, G.Q. Li, and Z.T. Sui, Precipitation selectivity of perovskite phase from Ti-bearing blast furnace slag under dynamic oxidation conditions, *J. Non-Cryst. Solids*, 353(2007), No. 22-23, p. 2214.
- [11] L.Y. Shi, Y.L. Zhen, D.S. Chen, Q. Tao, and L.N. Wang, Carbothermic reduction of vanadium–titanium magnetite in molten NaOH, *ISIJ Int.*, 58(2018), No. 4, p. 627.
- [12] Y.M. Zhang, L.Y. Yi, L.N. Wang, D.S. Chen, W.J. Wang, Y.H. Liu, H.X. Zhao, and T. Oi, A novel process for the recovery of iron, titanium, and vanadium from vanadium-bearing titanomagnetite: Sodium modification–direct reduction coupled process, *Int. J. Miner. Metall. Mater.*, 24(2017), No. 5, p. 504.
- [13] Y.M. Zhang, L.N. Wang, D.S. Chen, W.J. Wang, Y.H. Liu, H.X. Zhao, and T. Oi, A method for recovery of iron, titanium, and vanadium from vanadium-bearing titanomagnetite, *Int. J. Miner. Metall. Mater.*, 25(2018), No. 2, p. 131.
- [14] F.C. Meng, Y.H. Liu, T.Y. Xue, Q. Su, W.J. Wang, and T. Qi, Structures, formation mechanisms, and ion exchange properties of alpha-, beta-, and gamma-Na₂TiO₃, *RSC Adv.*, 6(2016), No. 113, p. 112625.
- [15] D.S. Chen, L.S. Zhao, Y.H. Liu, T. Qi, J.C. Wang, and L.N. Wang, A novel process for recovery of iron, titanium, and vanadium from titanomagnetite concentrates: NaOH molten salt roasting and water leaching processes, *J. Hazard. Mater.*, 244-245(2013), p. 588.
- [16] D.S. Chen, B. Song, L.N. Wang, T. Qi, Y. Wang, and W.J. Wang, Solid state reduction of Panzhihua titanomagnetite concentrates with pulverized coal, *Miner. Eng.*, 24(2011), No. 8, p. 864.
- [17] L.H. Zhou and F.H. Zeng, Statistical analysis of the effect of Na₂CO₃ as additive on the reduction of vanadic–titanomagnetite–coal mixed pellets, *Adv. Mater. Res.*, 97-101(2010), p. 465.
- [18] Z.H. Zhu, G.Q. Lu, and R.T. Yang, New insights into alkali-catalyzed gasification reactions of carbon: Comparison of Na₂O reduction with carbon over Na and K catalysts, *J. Catal.*, 192(2000), No. 1, p. 77.
- [19] E. Foley and K.P. Mackinnon, Alkaline roasting of ilmenite, *J. Solid State Chem.*, 1(1970), No. 3-4, p. 566.
- [20] V. Tathavadkar, and A. Jha, The effect of molten sodium titanate and carbonate salt mixture on the alkali roasting of ilmenite and rutile minerals, [in] VII International Conference on Molten Slags Fluxes and Salts, Cape Town, p. 255.
- [21] A. Lahiri, and A. Jha, Kinetics and reaction mechanism of soda ash roasting of ilmenite ore for the extraction of titanium dioxide, *Metall. Mater. Trans. B*, 38(2007), No. 6, p. 939.
- [22] S. Parirenyatwa, L. Escudero-Castejon, Y. Hara, A. Jha, and S. Sanchez-Segado, Comparative study of alkali roasting and leaching of chromite ores and titaniferous minerals, *Hydrometallurgy*, 165(2016), p. 213.
- [23] C. Li, A.F. Reid, and S. Saunders, Nonstoichiometric alkali ferrites and aluminates in the systems NaFeO₂–TiO₂, KFeO₂–TiO₂, KAlO₂–TiO₂, and KAlO₂–SiO₂, *J. Solid State Chem.*, 3(1971), No. 4, p. 614.
- [24] J.W. Kim and H.G. Lee, Thermal and carbothermic decomposition of Na₂CO₃ and Li₂CO₃, *Metall. Mater. Trans. B*, 32(2001), No. 1, p. 17.
- [25] C.W. Bale, P. Chartrand, S.A. Degterov, G. Eriksson, K. Hack, R. Ben Mahfoud, J. Melançon, A.D. Pelton, and S. Petersen, FactSage thermochemical software and databases, *Calphad*, 26(2002), No. 2, p. 189.
- [26] P.C. Holloway, T.H. Etsell, and A. L. Murland, Roasting of La Oroya zinc ferrite with Na₂CO₃, *Metall. Mater. Trans. B*, 38(2007), No. 5, p. 781.
- [27] P.C. Holloway, T.H. Etsell, and A.L. Murland, Use of secondary additives to control the dissolution of iron during Na₂CO₃ roasting of la oroya zinc ferrite, *Metall. Mater. Trans. B*, 38(2007), No. 5, p. 793.
- [28] E.N. Selivanov, K.V. Pikulin, L.I. Galkova, R.I. Gulyaeva, and S.A. Petrova, Kinetics and mechanism of natural wolframite interactions with sodium carbonate, *Int. J. Miner. Metall. Mater.*, 26(2019), No. 11, p. 1364.
- [29] R.Z. Xu, J.L. Zhang, W.X. Han, Z.Y. Chang, and K.X. Jiao, Effect of BaO and Na₂O on the viscosity and structure of blast furnace slag, *Ironmaking Steelmaking*, 47(2020), No. 2, p. 168.
- [30] A. Tomita, Catalysis of carbon–gas reactions, *Catal. Surv. Jpn.*, 5(2001), No. 1, p. 17.
- [31] W. Pan, Z.J. Ma, Z.X. Zhao, W. H. Kim, and D.J. Min, Effect of Na₂O on the reduction of Fe₂O₃ compacts with CO/CO₂, *Metall. Mater. Trans. B*, 43(2012), No. 6, p. 1326.